OPTIMIZING MACROPHAGE EXOSOMES FOR PAYLOAD DELIVERY AND EXTENDED STORAGE USING TARDIGRADE-DERIVED

By

Amani Gajjar

A capstone project submitted for Graduation with University Honors

May 06, 2026

University Honors

University of California, Riverside

APPROVED

Dr. Bahman Anvari

Department of Bioengineering

Dr. Begoña Echeverria, Howard H Hays, Jr. Chair

University Honors

ABSTRACT

Macrophages are innate immune cells responsible for engulfing foreign material and clearing damaged cells. They naturally migrate toward sites of inflammation, making them attractive candidates for targeted payload delivery. They also release exosomes, nanosized (30-150 nm) extracellular vesicles (EVs) of endosomal origin that retain key molecular features of their parent cell and protect selected cargo from premature degradation. Exosomes have emerged as versatile delivery vehicles across wound healing, inflammation, regeneration, and the blood-brain barrier. Indocyanine Green (ICG) is a near-infrared dye widely used in medical imaging and photothermal therapies but is limited by its half-life of ~3-5 minutes. Macrophages and their exosomes may enhance ICG circulation time and delivery. However, low exosome yield and ex vivo stability remain barriers to translational application of macrophage-derived exosomes. In this study, we established a reproducible macrophage exosome isolation protocol and confirmed particle size within the expected range using Dynamic Light Scattering and Scanning Electron Microscopy. Furthermore, to address the challenge of long-term exosome storage, we are investigating the incorporation of cytoplasmic abundant heat soluble (CAHS) proteins known to stabilize cellular structures under extreme conditions. Preliminary UV-Vis spectroscopy data has demonstrated the presence of CAHS protein within exosomes following macrophage CAHS expression, suggesting successful incorporation. This study aims to optimize ICG loading into macrophage-derived exosomes while also addressing exosome stability and storage. By refining loading strategies and CAHS-mediated preservation, these experiments seek to enhance the longevity, functionality, and translational potential of exosome-based delivery systems for imaging and therapeutic applications.

ACKNOWLEDGEMENTS

I would like to extend my deepest gratitude to my faculty-mentor, Dr. Bahman Anvari, for his invaluable guidance and unwavering support throughout this project. His expertise and constructive feedback were instrumental in shaping this work. I also wish to thank Dr. Begoña Echeverria and the entire University Honors team for their continuous support and for providing the framework and resources necessary to complete this capstone.

TABLE OF CONTENTS

Abstract 2

Acknowledgements 3

Table of Contents. 4

Introduction 5

Background and Literature Review. 6

Methods and Results 9

Conclusion. 33

References. 35

INTRODUCTION

Macrophages are vital components of the innate immune system, responsible for host defense, inflammation, and tissue homeostasis.[1] Their ability to migrate to sites of inflammation has led to extensive research into utilizing macrophages as cell-based therapeutic delivery vehicles. Furthermore, macrophages secrete exosomes (30-150 nm), extracellular vesicles (EVs) capable of delivering biological cargo.[2] Macrophage exosomes, which are secreted by both classically (M1) and alternatively (M2) activated phenotypes while maintaining many of the same surface markers and functions as their parent cells,[1] have recently emerged as promising candidates for drug delivery vehicles due to their biocompatibility, low immunogenicity, and efficient cell targeting capabilities.

One particular interest in this field is indocyanine green (ICG): a near-infrared fluorescent dye clinically approved for imaging and undergoing investigation for photothermal therapy.[3] With appropriate illumination, ICG can be used for tumor imaging with concomitant heat generation. Despite its approval for clinical use, ICG is limited by rapid hepatic clearance and a short half-life in circulation,[4] and there is an appeal to encapsulate ICG for improved retention and longer lasting imaging capability.

Initial strategies utilizing ICG-loaded macrophages have simply relied on cellular trafficking to deliver the ICG to a target location.[5] While uptake may be considerable, one major drawback is insubstantial retention. The loss of ICG signal over time and concurrent accumulation in the media observed in this study has previously been reported and reveals that biologically active or intracellularly localized ICG is not stably retained.[6]

These observations point to an issue informative of more than just loading: system stability. Even with ideal loading, a successful delivery system must maintain its function. With

this consideration, exosomes are advantageous over parental cell populations because, among other properties, they are smaller, less complex, and more easily sequester contents in their interior.[7] However, their stability as a delivery system presents further limitations.

A major factor contributing to this drawback is loss of exosome integrity during freeze-thaw,[8] making this an important property to consider for applications. Here, improved exosome production and stability were pursued. Exosomes were produced from macrophages via a previously reported method to stimulate their release and were confirmed to be within the appropriate size range. To stabilize the resulting exosomes, exosome production or storage was supplemented with cryoprotectants or proteins of the cytoplasmic abundant heat soluble (CAHS) family, which have been demonstrated to protect cells from these environmental stresses.[9]

Together, these data highlight a shift away from concerns regarding loading toward the challenge areas of stability, retention, and preservation. The focus of this work is to optimize the isolation of macrophage-derived exosomes and to stabilize them with the use of cryoprotectants and CAHS proteins for ICG application.

BACKGROUND AND LITERATURE REVIEW

Indocyanine green (ICG) is a near-infrared (NIR) fluorescent dye that has been widely used in clinic imaging with a strong absorption of NIR in the 700–800 nm range, which can penetrate through biological tissues.[10] Due to these optical features, it has been applied for angiography, sentinel lymph node mapping, and imaging of various tumors. In addition, ICG has also been intensively used in photothermal therapy to generate heat to kill specific cells when activated by light.[11] However, the rapid liver clearance and short circulation half-life after intravenous injection severely limit its broad bio-applications.[4]

To overcome these shortages, many nanocarriers, such as liposomes and synthetic polymer-based nanoparticles encode ICG to improve its stability and prolong its half-life.[12] However, these artificial carriers are easily uptaken by the reticuloendothelial system (RES), have limitations due to their possible toxicity, tampered targeting abilities, and tedious preparation procedures.[13] Biological drug delivery systems for ICG are thus developed aiming at improving its tissue targeting and cell-specific delivery without inducing toxicity.

Exosomes have attracted attention as a credible substitute for synthetic carriers. They are typically 30-150 nm in diameter and naturally produced by cells.[7] Instead of pure proteins or lipids, exosomes have a highly organized structure with proteins and lipids distributed non-randomly. These vesicles provide means of intercellular communication by transferring proteins, lipids and genetic material, and they are also found in biological fluids such as milk, urine, blood, saliva and cerebrospinal fluid, etc.[14] Of note, exosomes inherit a number of features from their parent cells. They are non-immunogenic, nontoxic, extremely stable in blood circulation, and have a long half-life. They thus have great potential for drug delivery and imaging.[7]

Recently, researchers have successfully manipulated exosomes for the delivery of cargo molecules.[15] Compared with conventional nanocarriers such as liposomes, exosomes have superior capabilities for stabilizing their cargo molecules, increasing their circulation time and enhancing cellular uptake.[7,15] It is found that molecules carried by exosomes are protected from enzymatic degradation, and exosomes can even deliver cargo to the brain by mediating transport across the blood-brain barrier.[15,16] Encapsulating ICG in exosomes might likewise increase its stability and retention. Despite these advantages, the encapsulation efficiency and tissue targeting abilities of exosome mediated delivery need to be improved.[15]

Macrophage-derived exosomes are particularly interesting for their natural function and targeting ability. In nature, can home in on inflammatory and cancer sites, and the activation state of the source macrophages correlates to the signaling activity of exosome cargo;[5,17] thus, they are able to perturb their environment. Despite these advantages, there are still many barriers to overcome before these systems can be transformed into reliable platforms.

First is the problem of poor cargo loading and retention. The most common methods for loading exosomes are passive (incubation at 37°C), or active by electroporation.[15] Despite many methods for loading vesicles with cargo, even after loading it is difficult to achieve long-term retention, especially for small-molecule cargoes like ICG.

Moreover, isolation of exosomes is itself a challenge. For instance, isolation via the most common technique of differential ultracentrifugation is not always reproducible, can yield heterogenous populations of vesicles, and is often associated with contamination by non-exosome proteins or other extracellular vesicles.[18]

Stability of exosomes during storage is another major challenge, since exosomes are highly affected by freeze-thaw cycles that can disrupt the membrane and promote vesicle fusion, changing their size distribution pattern, as well as aggregated, resulting in a loss of function.[8] These events are even more frequent when exosomes are stored in standard buffers (e.g. PBS) that offer no protection against ice crystals.[19]

One way researchers have tried to address this issue is to incorporate various cryoprotective agents. This has been widely investigated, and sucrose and trehalose are known to stabilize lipid bilayers by forming a matrix around the vesicles that diminishes mechanical stress and reduces aggregation upon freezing.[20,21] Most recently, inspiration has been drawn from biological systems. Cytoplasmic abundant heat soluble proteins (CAHS), which can be isolated

from tardigrades, have been associated with cellular stabilization during hydration and freezing stresses.[21]

The current literature collectively demonstrates that exosomes serve as a promising delivery platform for ICG, yet they also possess their own limitations. This thesis combines the improvements made to isolation methods for exosomes and the use of stabilizing mechanisms for exosomes with the use of cryoprotectants as well as CAHS proteins in future directions.

METHODS AND RESULTS

The methodology presented in this thesis spans several academic quarters and evolved from exploratory work in near-infrared erythrocyte-derived transducers, macrophage culture, and protein-loading experiments into a more concentrated study on macrophage-derived exosome isolation, indocyanine green loading, and exosome stabilization in the presence of synthetic and biologic proteins. The research timeline began in my sophomore year with introductory macrophage culture and NET fabrication work, moved toward exosome isolation in Winter 2025, expanded into ICG loading and retention studies in Spring 2025, and continued into my junior year with exosome storage, CAHS protein incorporation, LPS stimulation, and post-freeze stability analysis.

Macrophage Culture Establishment and NET Fabrication (Fall 2024)

During Fall 2024, the first half of this project consisted of training in key laboratory procedures: in this case, passaging of RAW 264.7 macrophages and fabrication of NETs. While RAW macrophages would eventually form a key part of the capstone project, here they served as training tools and were cultured in parallel with NET fabrication.

RAW macrophages were cultured and passaged. Media was aspirated and replaced with new DMEM media. When cells reached appropriate confluency, they were trypsinized and

pelleted by centrifugation at ~500 ×g. The supernatant was aspirated before the cells were resuspended in new media and re-plated. This cycle of centrifugation and supernatant aspiration would be important training for generating reproducible results.

In parallel, NETs were fabricated as a continuous process alongside a PhD student. Multiple rounds of NET preparation were completed. The protocol involved many rounds of centrifuging the sample and keeping or discarding the supernatant.

This process took several weeks due to the 24 hour waiting period during key protocol steps. This process was restarted several times to improve batch consistency. During this time, macrophages were maintained in culture. Preparation of NETs and macrophage cultures in parallel served as key training for later protein-loading and especially exosome experiments, as the process of spinning down and separating materials after centrifugation would be key to isolation.

Exosome Isolation and Hypotonic Release Protocol Development (Winter 2025)

During Winter 2025, the experimental focus shifted from initial protein-loading studies to macrophage-derived exosome isolation protocols, forming the central direction of the Honors Capstone. At the beginning of the quarter, progress was guided by milestones that included macrophage culture expansion, and preparation for protein-loading experiments based on electroporation and subsequent optimization of protein concentration, voltage, and time-incubation parameters.

Around Week 3, after discussion of goals for the Honors Capstone and input from my affiliated faculty mentor, the focus of the project shifted towards an exosome-based delivery system. This shift was motivated by the fact that although intracellular ICG loading could be performed, the dye would leak out of the cell within hours, rendering it ineffective for longer-

term uses. The focus thus shifted from optimizing intracellular ICG loading to developing macrophage-derived exosomes with improved retention of their cargo based on a literature review performed during Weeks 3-4. A particular emphasis was on hypotonic stimulation of macrophages to induce extracellular vesicle release.

Informed by this review, a hypotonic exosome isolation protocol was chosen.[22] DMEM media was prepared as recommended. Base DMEM was supplemented with 10% (v/v) fetal bovine serum (FBS) and 1% (v/v) penicillin–streptomycin to produce Complete DMEM. It was mixed together under sterile conditions and kept at 4°C before use. The RAW macrophages were grown to high density before starting this procedure to increase vesicle yield. Complete DMEM was brought to 37°C before use on cells. The previous cell culture media was aspirated, and the cells were given a hypotonic media composed of 3mL complete DMEM and 7mL nanopure water (ratio 3:7). The cultures were incubated with 10mL hypotonic media for 30 minutes.

After incubation, the media was collected and spun down according to the following differential centrifugation protocol (Figure 1): The media was first centrifuged at 500 ×g for 5 minutes to pellet intact cells. The supernatant was transferred to a new tube and centrifuged at 2,000 ×g for 10 minutes to pellet dead cells, then at 10,000 ×g for 30 minutes to pellet larger cellular debris. In between each spin, the supernatant was separated from the pellet fraction in a new tube to avoid contamination. The clarified media solution was then ultracentrifuged at 90,000 ×g for 70 minutes. This produced a pellet of exosome-like vesicles as well as co-isolated proteins. The supernatant was aspirated, and the pellet was resuspended in PBS to perform a wash step.[22]

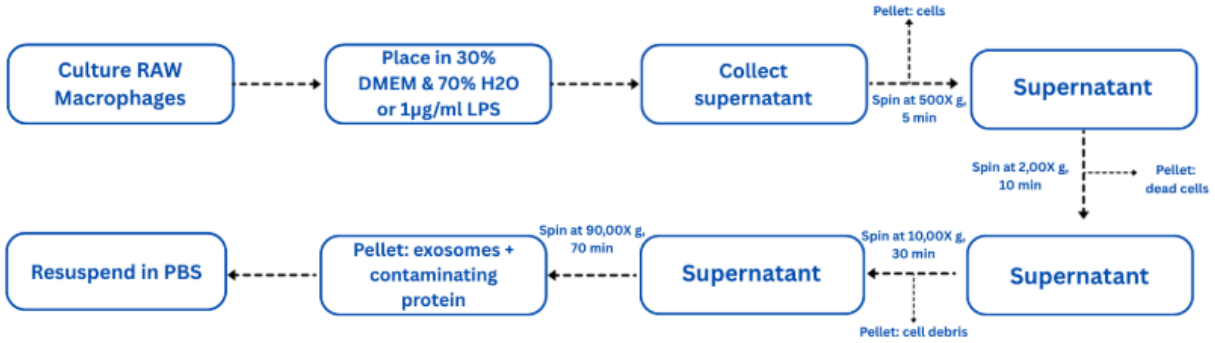

Figure 1. *Exosome isolation workflow from RAW macrophage cultures.*

Initial experiments utilized macrophage cultures plated to extreme overconfluence, in order to obtain the largest possible amount of vesicles. Cell culture media was harvested directly from overgrown plates. Purification appeared to be successful as a pellet was visible following ultracentrifugation of the sample particularly during Week 6. However, it was difficult to confirm purification of exosomes due to the nanometer scale of vesicles as well as contamination by free protein. The 10,000 ×g centrifugation step did not result in a visible pellet in any of the purifications, suggesting that this step may be non-essential to successful purification and can be avoided in the future.

The isolation procedure was performed again during Weeks 10-11 using the same hypotonic stimulation and centrifugation workflow. Dynamic light scattering was employed to characterize whether the isolated material was within the size range of exosomes. A fairly large proportion of the particle size distribution lies within the expected size range for exosome-type vesicles (~30–150 nm).

In parallel with experimental development, the research direction was formalized through the drafting of the initial capstone abstract, which detailed the reasoning for using macrophages and macrophage-derived vesicles to deliver ICG. Briefly, it was hypothesized that exosomes would be able to deliver increased amounts of ICG to areas of interest by preventing its rapid

clearance, since this was suspected to be the driving force behind poor retention of the free chromophore. In the following weeks, the project began to focus on optimizing exosome isolation in preparation for the eventual pairing with ICG-loading experiments.

In parallel, continuous documentation of experimental progress detailed iterative modifications to the isolation protocol, noting changes in yield and purity and highlighting major limitations such as possible protein contamination and stability. This feedback informed continued development of both the exosome isolation protocol and macrophage-based experimental workflows over the quarter.

Dynamic light scattering (DLS) was used to analyze particles isolated by hypotonic stimulation and differential ultracentrifugation.[22] The number distribution (Figure 2a) indicates that the majority of the particles are in the nano-size range (1-100nm), and thus this protocol successfully isolates exosome-sized particles. The volume distribution (Figure 2b), on the other hand, highlights peaks at much larger sizes in the micron range, which most likely result from aggregated particles.

(a)

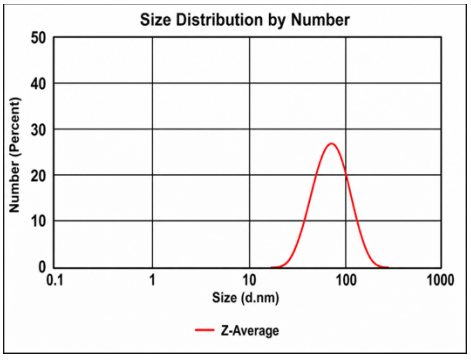

(b)

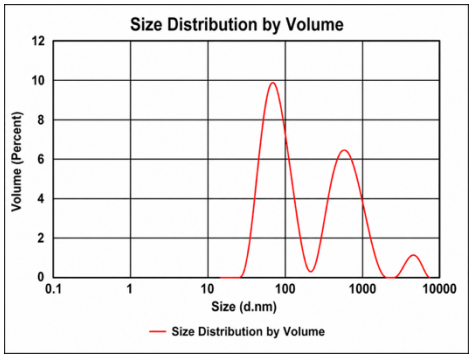

Figure 2. *Dynamic light scattering (DLS) characterization of particles isolated following hypotonic stimulation and ultracentrifugation.* ***(a)*** *Number distribution of particle size.* ***(b)*** *Volume distribution of particle size.*

Optimizing ICG Loading and Evaluating Intracellular Retention Dynamics (Spring 2025)

This quarter, my research focused on optimizing intracellular loading and retention of Indocyanine Green (ICG) in immune cells for potential applications in photothermal therapy. I tested various ICG concentrations and incubation times across multiple immune cell types, including parental RAW 264.7 macrophages, MAHS-expressing RAW 264.7 macrophages, and Thp-1 monocytes. The main goals were to identify loading conditions that maximize ICG uptake while preserving cell viability, and to determine the stability of ICG inside cells post-loading.

Over the course of the quarter, I conducted a series of experiments to evaluate these parameters. This included microscopy imaging before and after ICG loading, absorbance and fluorescence measurements at 0 and 24 hours, and a full 24-hour time-resolved experiment to determine when ICG begins to leak from monocytes into the surrounding media. Additional work involved working with Grant and Tashdid on thermal profiling of loaded macrophages under laser exposure and comparing the temperature response between MAHS and AcGFP expressing cells. Collectively, these studies provided insight into ICG behavior across cell types and time points, forming the basis for future work aimed at improving intracellular dye retention.

<u>ICG Loading Protocol Development and Initial Trial in RAW Macrophages (Week 2)</u>

During Week 2, I initiated ICG-loading experiments using standard RAW 264.7 macrophages to determine the optimal combination of ICG concentration and incubation time. I began by thawing a cryopreserved vial of macrophages in a 37°C water bath and transferred the contents into a sterile tube containing pre-warmed DMEM. The cells were centrifuged at 400g for 5 minutes, after which the supernatant was aspirated, and the cell pellet was resuspended in 5 mL of fresh media. To seed the 96-well plate with a target density of 2 × 104 cells per 100 µL per well, I began with a cryovial containing approximately 1 × 106 cells per mL. Assuming no

loss of cells, I performed a two-step dilution process to achieve the desired concentration. First, I prepared Solution 1 by adding 1 mL of the original cell suspension into 5 mL of pre-warmed DMEM, resulting in a concentration of 0.2 × 106 cells/mL, or 2 × 105 cells/mL. Next, I prepared Solution 2 by taking 1 mL of Solution 1 and diluting it into 10 mL of media. This final dilution brought the concentration to 2 × 104 cells per 100 µL, which matched the seeding requirement for each well of the plate. I then plated 100 µL of this diluted suspension into each well.

Next, I prepared ICG working solutions using a 2.56 mM stock to create a range of concentrations: 100 µM, 200 µM, 400 µM, 600 µM, 800 µM, 1.0 mM, and 1.1 mM. For each concentration, I calculated the volume of ICG stock and DMEM needed to reach a final volume of 100 µL per well (e.g., 100 µM = 4 µL ICG + 96 µL DMEM; 1.1 mM = 44 µL ICG + 56 µL DMEM). I applied each concentration to the plated cells and incubated for 30 minutes, selecting this duration as the initial time point from a broader list of planned incubation intervals ranging from 30 minutes to 6 hours.

Following the incubation, I evaluated intracellular ICG uptake using PBS-based absorbance measurements and microscopy. The 1.1 mM sample loaded for 30 minutes showed very little dye internalization under the microscope, indicating poor ICG loading. Based on these findings, we concluded that 30 minutes was insufficient for effective ICG uptake and decided to test longer incubation durations. The revised time points included 60 minutes, 90 minutes, 2 hours, 3 hours, 4 hours, 5 hours, and 6 hours. Additionally, absorbance spectra for Day 0 samples of 0.3, 0.6, and 1.1 mM ICG, shown in Figure 3, revealed peaks in the 550-600 nm range, consistent with the absorbance profile of DMEM. This suggested that some supernatant remained in the wells despite initial washing. Because the DMEM contained residual ICG from the loading step, the resulting absorbance data reflected both intracellular and extracellular dye,

making it unreliable for interpreting true cellular uptake. As a result, we implemented an additional PBS washing step in all subsequent experiments to minimize media interference.

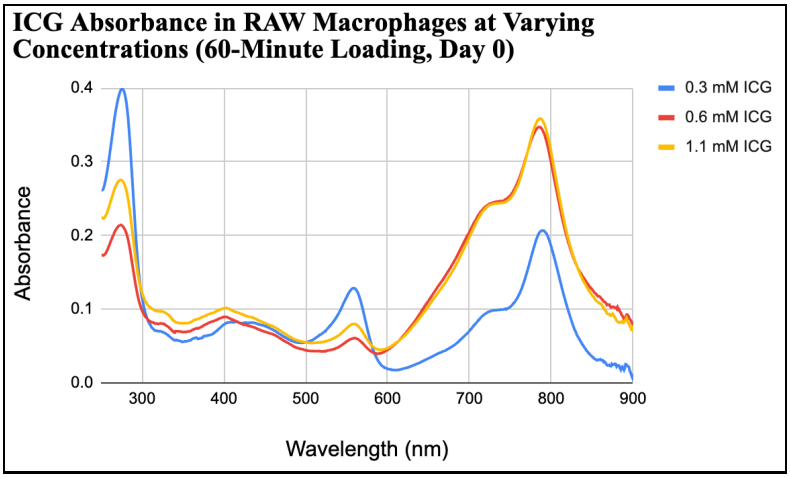

Figure 3. *Absorbance spectra of RAW macrophages loaded with 0.3 mM, 0.6 mM, and 1.1 mM ICG for 60 minutes, measured immediately after loading (Day 0). Peaks near 550–600 nm are attributed to residual DMEM in the samples.*

ICG Loading in MAHS-Expressing Macrophages and Microscopy Assessment (Week 3)

In Week 3, I began testing ICG loading in MAHS-expressing macrophages to compare their uptake and retention capacity with standard RAW 264.7 macrophages. I applied ICG concentrations ranging from 0.1 mM to 1.1 mM across incubation times spanning 20 minutes to 6 hours. The primary objective was to determine the ideal loading time and concentration based on both absorbance and cell viability. To visually assess the intracellular distribution of ICG, I captured microscopy images at two time points: Day 0 (at 10× and 25× magnification) and Day 1 (25× magnification). These images confirmed ICG presence in several conditions and are presented in Figure 4a (Day 0, 10×), Figure 4b (Day 0, 25×), and Figure 4c (Day 1, 25×).

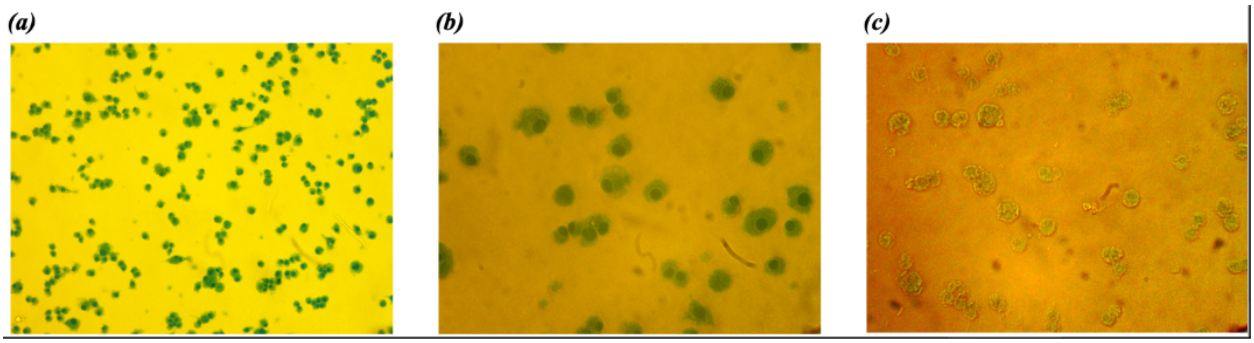

Figure 4. *Microscopy images of MAHS-expressing macrophages loaded with 1.1 mM ICG.* ***(a)*** *10× and* ***(b)*** *25× magnification immediately after loading;* ***(c)*** *25× magnification at 24 hours post-loading.*

ICG Retention in RAW Macrophages Over 24 Hours (Week 5)

Building on the previous experiments, we identified that loading RAW macrophages with 1.1 mM ICG for 1 hour produced consistent absorbance and visual confirmation of intracellular uptake. While this time point and concentration pair is effective, we had concerns about the stability of the loading.

To verify proper loading, we took microscopy images of RAW macrophages before ICG exposure (Figure 5a), immediately after 1-hour incubation with 1.1 mM ICG (Figure 5b and 5c), and again 24 hours post-loading (Figure 5d and 5e). The images showed a noticeable decrease in ICG intensity after 24 hours, suggesting that ICG may have either leaked into the surrounding media, degraded inside the cells, or both.

To determine if the ICG was leaking into the media or degrading over time, we measured the absorbance of the cells after 1 hour and again after 24 hours (Figure 6a). The absorbance dropped significantly after 24 hours, matching what was seen in the images. We then measured fluorescence and found that while the 1-hour sample showed a strong signal, the 24-hour sample showed almost no fluorescence (Figure 6b), reinforcing the conclusion that ICG levels in the cells decreased over time.

To rule out any interference from residual media, we also recorded the absorbance spectrum of DMEM, which confirmed it was not responsible for any peaks seen in the cell

samples (Figure 7). To further determine whether ICG is leaking or degrading, we now need to measure the absorbance of the surrounding media after 24 hours and evaluate ICG's stability at 37°C under identical conditions.

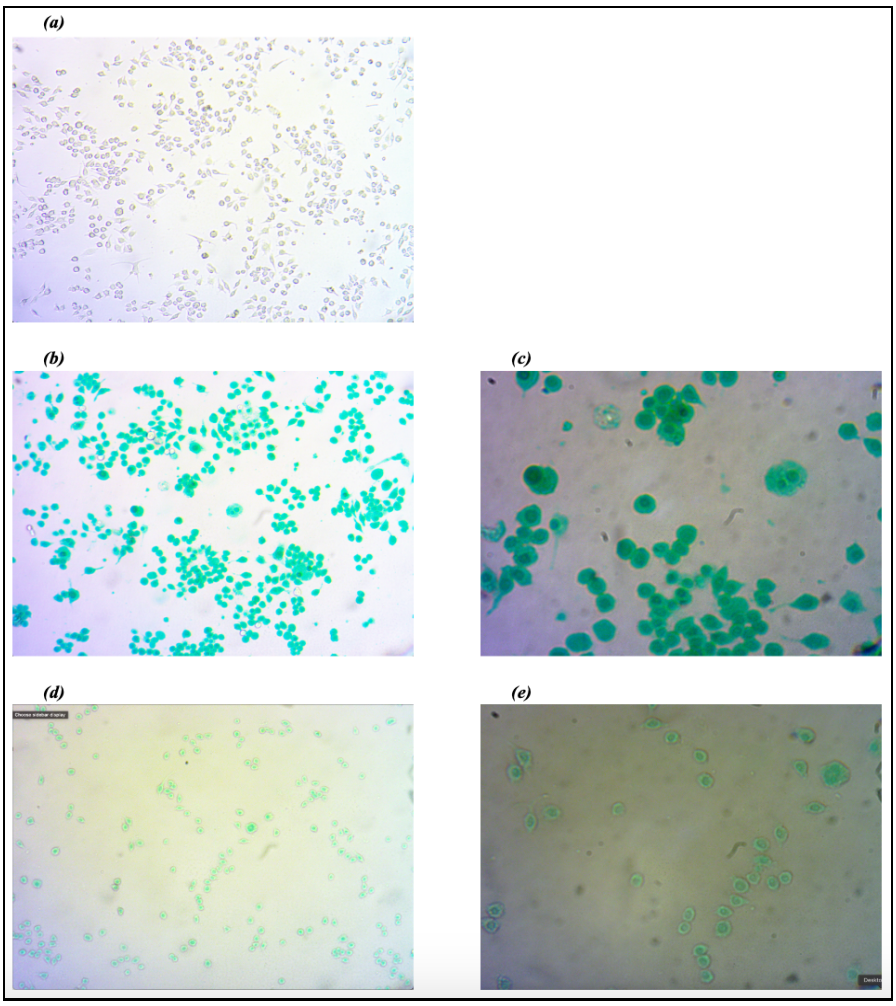

Figure 5. *Microscopy images of RAW macrophages before and after 1-hr loading with 1.1 mM ICG.*

- ***(a)*** *Pre-loading, 10× magnification. Cells show no visible fluorescence or dye accumulation*
- ***(b)*** *Immediately post-loading, 10×. Cells show widespread ICG uptake across cell populations*
- ***(c)*** *Immediately post-loading, 25×. Cells show strong intracellular ICG uptake.*
- ***(d)*** *24 hours post-loading, 10×. Cells show reduced ICG signal compared to* ***(b)****.*
- ***(e)*** *24 hours post-loading, 25×. Cells show reduced ICG signal compared to* ***(c)****.*

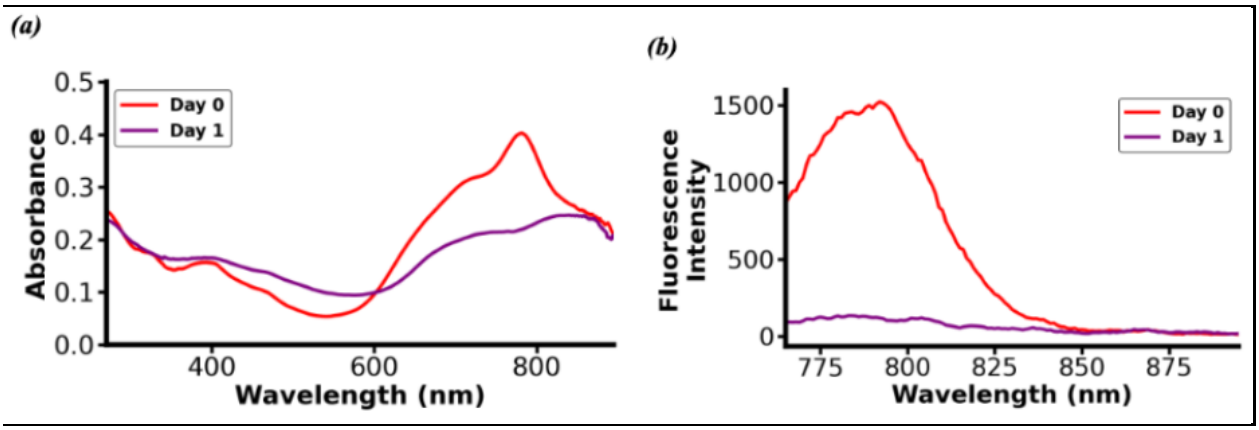

Figure 6. (a) *Absorbance spectra of RAW macrophages loaded with ICG for 1 hour, measured at 0 hours and 24 hours post-loading.* ***(b)*** *Fluorescence of RAW macrophages loaded with ICG for 1 hour, measured at 0 hours and 24 hours post-loading, showing strong signal at 0 hours and near-complete loss after 24 hours.*

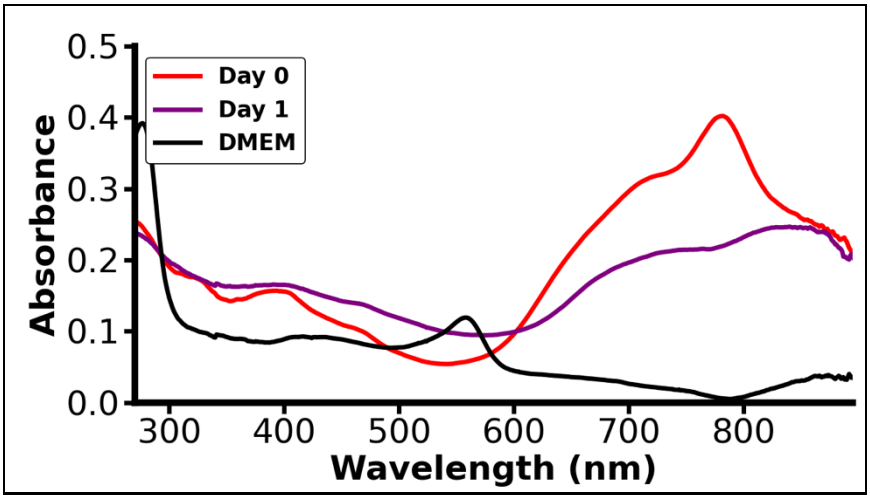

Figure 7. *Absorbance spectrum of DMEM alongside absorbance spectra of RAW macrophages at 0 hours and 24 hours post-loading. Confirms that DMEM does not interfere with or contribute to observed ICG peaks.*

Transition to Monocytes and Confirmation of ICG Leakage (Week 6)

Following past observations and results, we inferred that ICG was either degrading inside the macrophages or leaking into the media. To confirm this, we measured the absorbance of the media collected 24 hours after ICG loading. The spectrum showed a clear ICG peak, confirming that the dye had exited the cells and accumulated in the surrounding media, similar to what was later observed with monocytes in Figure 8a.

Based on this outcome and my faculty mentor's recommendation, our experiments were redirected to monocytes, since they are more therapeutically relevant. We measured the absorbance of three groups: monocytes before ICG loading, monocytes immediately after 1-hour loading with 1.1 mM ICG, and the same monocytes 24 hours loading.

As seen in Figure 8a, the Day 0 monocytes (immediately after loading for 1 hour with 1.1mM ICG) showed a distinct ICG absorbance peak, but the Day 1 sample closely resembled the absorbance of the untreated monocytes. This strongly suggests that, just like with the macrophages, ICG was either leaking out of the monocytes or being degraded intracellularly.

To investigate further, we measured the absorbance of the supernatant from the 24-hour post-loading monocyte wells. As shown in Figure 8b, the media had a strong ICG absorbance peak, confirming that the dye had leaked from the cells into the surrounding media. These results highlighted a consistent trend of ICG loss across both cell types.

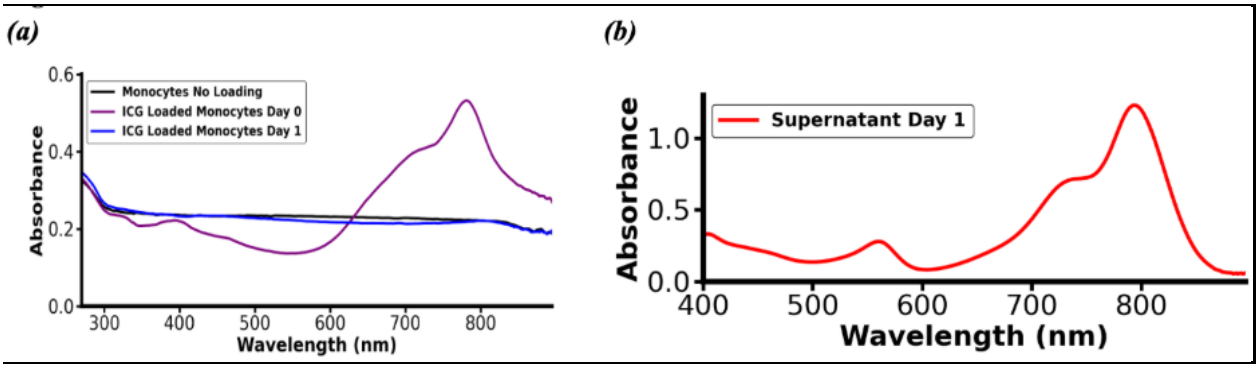

Figure 8. (a) *Absorbance spectra of monocytes loaded with ICG for 1 hour, measured at 0 hours (Day 0) and 24 hours (Day 1) post-loading.* ***(b)*** *Absorbance of the supernatant collected from ICG-loaded monocytes 24 hours after loading, showing a strong ICG signal in the media.*

Time-Resolved Study of ICG Leakage in Monocytes (Week 7)

Following confirmation that ICG consistently leaked out of both macrophages and monocytes after 24 hours, my faculty mentor suggested we observe when during the 24 hours this loss occurred. To address this, we designed a time-resolved experiment to track ICG leakage

and intracellular retention across a full day. Two 6-well plates of monocytes were prepared, both loaded with 1.1 mM ICG for 1 hour. Cells were then washed and resuspended in complete media. Plate 1 was measured at 0, 2, 4, 6, 8, 10, and 24 hours, while Plate 2 was measured at 0, 12, 14, 16, 18, 20, and 22 hours. This setup allowed us to track when ICG left the cells over 24 hours.

Figure 9 illustrates the gradual loss of ICG from monocytes over a 24-hour period. Media absorbance increased steadily, confirming continuous leakage rather than a single release event. Although intracellular ICG remained detectable up to 14 hours, the signal declined substantially by this point, indicating that most of the loss occurs within the first half of the time window. By 24 hours, a slight measurable amount of ICG remained in monocytes.

While monocytes showed slightly improved ICG retention compared to macrophages, the overall loss remained substantial. These findings suggest that passive loading alone may be insufficient for long-term retention. Other PhD students' electroporation experiments yielded more complete intracellular retention of ICG, supporting electroporation as a more effective strategy. Future experiments will focus on optimizing electroporation conditions to improve intracellular stability.

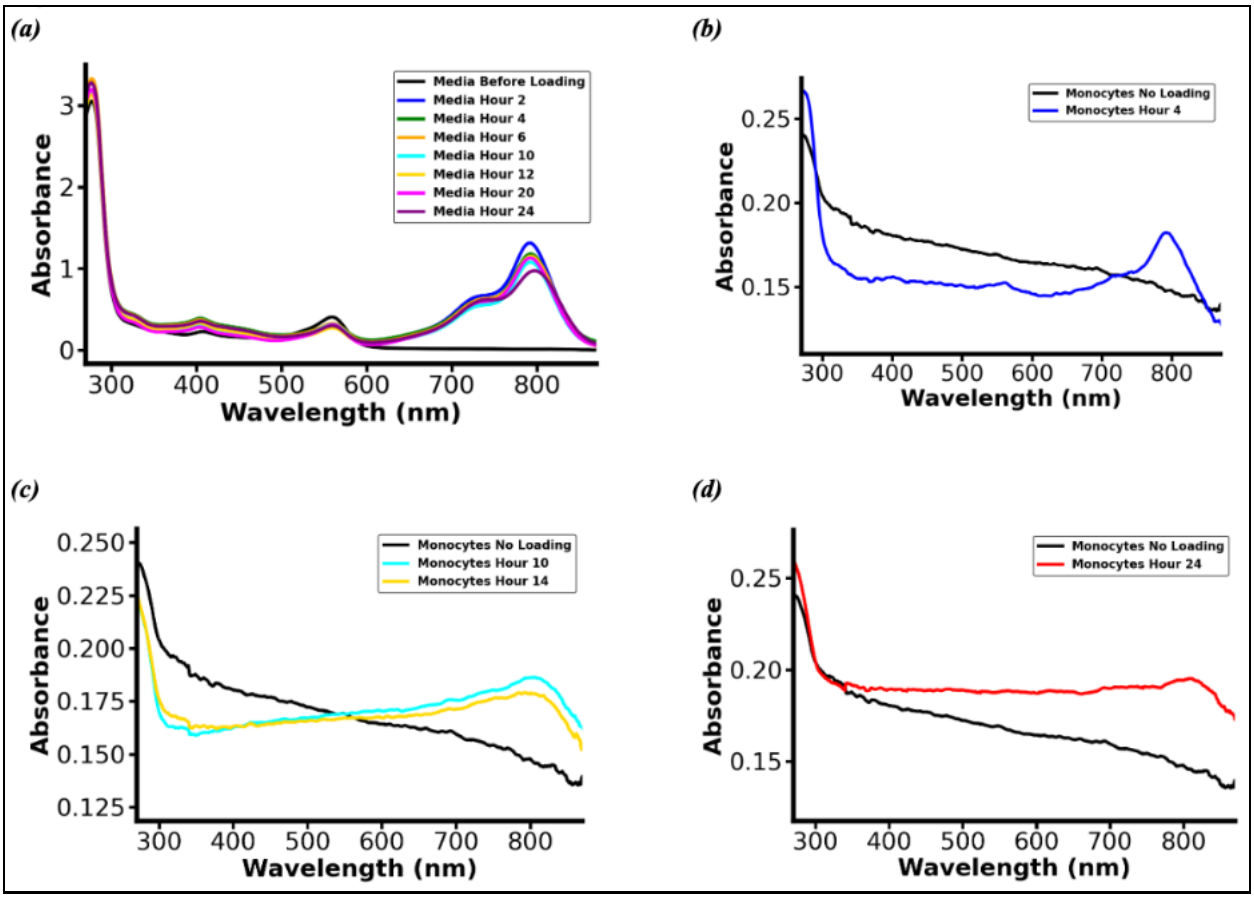

Figure 9. *Time-resolved absorbance analysis of ICG-loaded monocytes to assess intracellular retention and leakage.*

- ***(a)*** *Media absorbance at 2, 4, 6, 10, 12, 20, and 24 hours post-loading. Increase in ICG absorbance indicates leakage over time.*
- ***(b)*** *Absorbance of monocytes at 10 and 14 hours post-loading, compared to control. Shows progressive reduction in intracellular ICG.*
- ***(c)*** *Absorbance of monocytes at 4 hours post-loading, compared to unloaded control. Indicates early-stage ICG loss.*
- ***(d)*** *Absorbance of monocytes at 24 hours post-loading, compared to unloaded control. Some ICG signals remain, more than in macrophages.*

Thermal Response of RAW MAHS vs. AcGFP Macrophages (Week 9)

In Week 9, I assisted two PhD students in culturing and incubating RAW MAHS-expressing macrophages and RAW AcGFP macrophages for thermal response analysis under laser exposure. Figure 10a shows the thermal profile of RAW MAHS macrophages under laser exposure, with a rapid temperature rise to a little over 52°C followed by gradual cooling. In

Figure 10b, RAW AcGFP macrophages reached a slightly higher peak (~58°C), also followed by a steady decline.

The goal was to compare the photothermal profiles and evaluate whether MAHS-expressing macrophages might better tolerate thermal stress under laser exposure compared to AcGFP controls. However, the results showed no clear thermal protection advantage in the MAHS group, and cell survival outcomes did not favor MAHS over AcGFP.

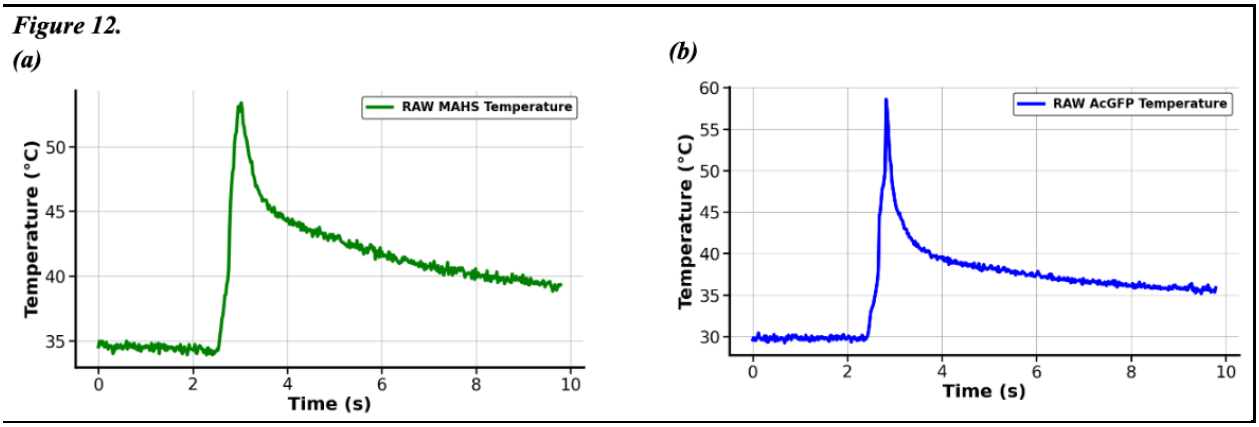

Figure 10. (a) *Temperature profile of RAW MAHS macrophages during laser exposure. The temperature peaks near 52.5 °C and gradually cools over time.* ***(b)*** *Temperature profile of RAW AcGFP macrophages under the same conditions. The peak reaches approximately 58.5 °C, slightly higher than in MAHS cells, followed by a similar cooling pattern.*

Exosome Isolation, ICG Incorporation, and Storage Protocol Development (Fall 2025)

In Fall 2025, experimental work was concentrated on bringing macrophage expansion, exosome isolation, ICG incorporation, CAHS-associated exosome generation, and early-stage storage optimization into a single work flow. This phase was the first concerted effort to take intracellular ICG incorporation to the next step and test whether macrophage-derived exosomes could be isolated, associated with ICG, and stored for later analysis of ICG stability.

RAW macrophages and AcGFP-expressing macrophages were expanded to prepare for exosome isolation. Cells were plated in T75 flasks and then transferred into T175 flasks when enough cells existed to reach 90% confluency in the corresponding larger surface area. This

expansion was done until there was enough conditioned media to use for exosome isolation, in concert with ICG incorporation experiments.

In Week 3, exosome isolation and ICG incorporation were first combined using a hypotonic stimulation protocol. ICG was prepared in nanopure water and added directly to macrophage cultures. For the control RAW macrophage condition, cultures were exposed to a hypotonic solution consisting of 12 mL complete DMEM and 28 mL H_2O containing ICG, corresponding to a 3:7 DMEM-to-water ratio or 30% DMEM and 70% H_2O. Cultures were incubated for 30 minutes to promote vesicle release. The collected supernatant was then processed through sequential centrifugation at 500 ×g for 5 minutes, 2,000 ×g for 10 minutes, and 10,000 ×g for 30 minutes to remove intact cells, dead cells, and larger debris. The clarified supernatant was then ultracentrifuged at 90,000 ×g for 70 minutes to pellet exosome-like vesicles. Following ultracentrifugation, green-blue pellets were visible in the ICG-treated samples, suggesting that ICG-associated material was retained in the isolated fraction (Figure 11). These pellets were subsequently evaluated using DLS measurements to assess particle size distribution and absorbance measurements to assess ICG association.

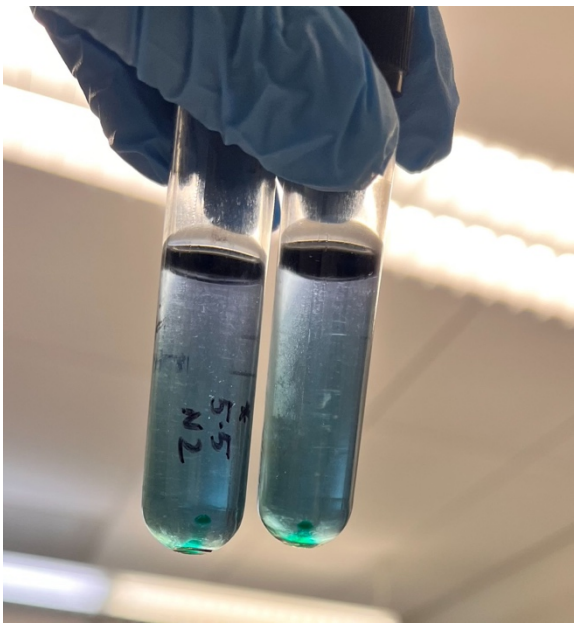

Figure 11. *Visible pellet formation (green circle on bottom of tube) following ICG-associated exosome isolation. The green-blue color of the pellet region suggests retention of ICG-associated material in the isolated fraction.*

In Week 4, the same workflow was executed using AcGFP-expressing macrophages in order to test whether a protein-associated signal could be detected in the final, exosome-containing pellet (Figure 12). This was a useful intermediate to CAHS-associated exosome experiments, since if AcGFP-associated material was not able to be detected, it was less likely that CAHS association with exosomes would be detectable under these experimental conditions. The same hypotonic ICG exposure and 500xg, 2,000xg, 10,000xg, and 90,000xg spins were performed, and isolated samples were stored in 50 mM trehalose, a common cryoprotectant, as a first-pass stabilization condition.[20]

In tandem, CAHS-associated exosome experiments were prepared using RAW 264.7 macrophages modified to express CAHS constructs. In this case, CAHS (Cytoplasmic Abundant Heat Stable) proteins derived from tardigrade stress-tolerance proteins were incorporated into RAW macrophages via the Sleeping Beauty transposon/transposase platform,[21,23] and antibiotic resistance was used to support selection of successfully modified cells (Figure 13). Once CAHS-expressing macrophages were established, they served as the source cells for exosome stimulation and isolation. Therefore, the resulting population of exosomes would be associated with the CAHS protein in a similar fashion to how the control exosomes are associated with AcGFP, supporting a comparison of CAHS-associated with control exosome preparations during post-freeze analysis.

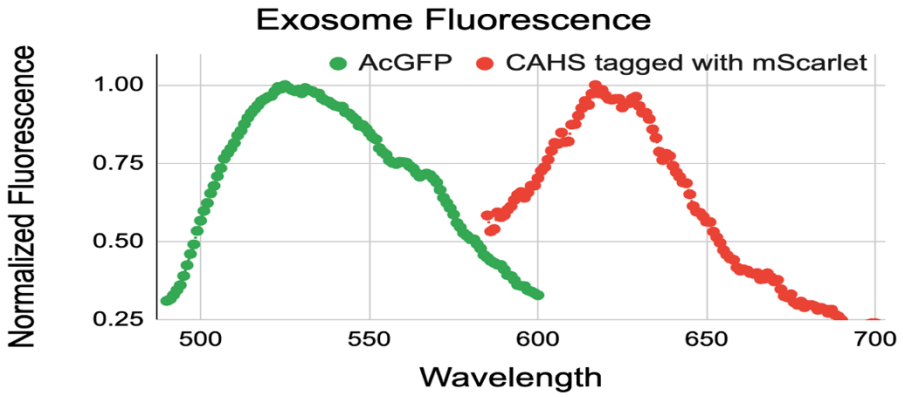

Figure 12. *Characterization of AcGFP control and CAHS-associated exosome samples. Fluorescence spectra comparing AcGFP control exosome samples with CAHS-associated exosome samples. AcGFP control exosome samples exhibited fluorescence consistent with the AcGFP signal, while CAHS-associated exosome samples exhibited fluorescence consistent with the CAHS-linked reporter signal, supporting the presence of protein-associated material in isolated exosome fractions.*

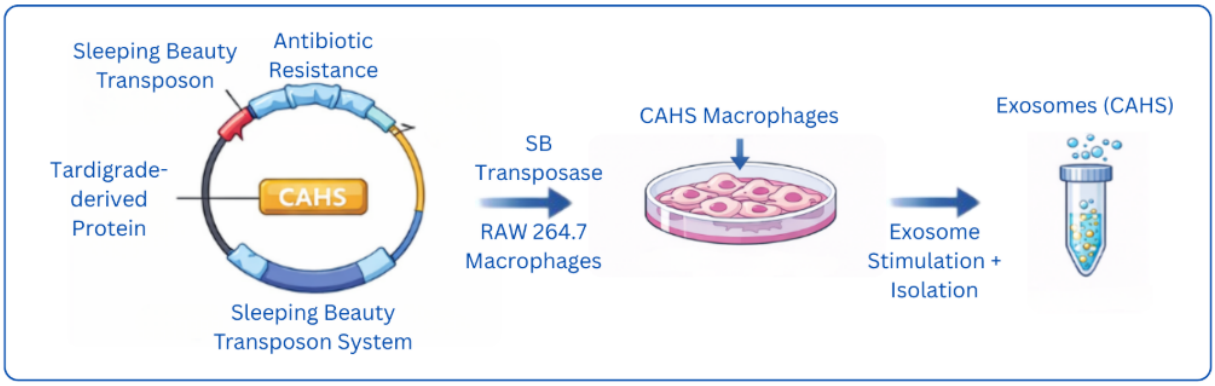

Figure 13. *Schematic representation of the Sleeping Beauty transposon-based system used to generate CAHS-expressing RAW 264.7 macrophages. A tardigrade-derived CAHS construct was introduced into macrophages using the Sleeping Beauty transposon and SB transposase system, with antibiotic resistance supporting selection of modified cells. CAHS-expressing macrophages were then to be used for exosome stimulation and isolation to generate CAHA-associated exosome samples for future stability analysis.*

During this same round of experiments, initial storage/cryopreservation conditions were established for later post-freeze comparison. After isolation by ultracentrifugation, exosome samples were allocated to two storage conditions. One utilized PBS only, while the other utilized a sucrose-based cryoprotectant prepared by dissolving 0.085 g sucrose in 1 mL of PBS (8.5% sucrose in w/v).[8] This also corresponded to an intended 100:1 (w/w) sucrose:protein ratio. Sucrose-containing samples were placed into a controlled-rate freezing container filled with

isopropyl alcohol to allow gradual cooling at 1 degree C per 10 minutes until reaching -80°C, at which point they were designated for long-term storage. PBS-only samples were used for immediate DLS characterization to determine initial particle size before freezing. The post-freeze results of this initial storage scheme, comparing sucrose with PBS preservation, were collected in Spring 2026 and are shown later (Figure 20).

Complete DMEM preparation was also standardized during this phase to improve consistency across experiments. Complete media was prepared by supplementing 500 mL basal DMEM with 50 mL fetal bovine serum and 5 mL penicillin–streptomycin, producing a final composition of approximately 89% DMEM, 10% FBS, and 1% penicillin–streptomycin.

By the end of Fall 2025, a working exosome isolation and ICG-association protocol had been established, AcGFP-expressing macrophages had been incorporated as a model for later protein-associated vesicles, a CAHS-expressing macrophages system had been generated for downstream use in CAHS-associated exosome experiments, and the first storage comparison between PBS and sucrose-based cryoprotection was established. Furthermore, the sucrose and PBS storage conditions compared during this quarter were not fully evaluated right away, but rather their post-freeze preservation was measured in Spring 2025 by DLS analysis. Therefore, this round of experiments was largely set up for storage and stability results, and post-freeze comparison data is available for them in Spring 2026 to indicate whether sucrose aided exosome preservation in this set of experiments.

LPS-Induced Exosomes and CAHS-Associated Stability Experiments (Winter 2026)

During Winter 2026, experimental efforts focused on refining macrophage-derived exosome production by comparing stimulation conditions and incorporating CAHS-associated systems into the workflow. This phase built on the exosome isolation and storage protocols

developed in Fall 2025 but shifted toward evaluating whether macrophage activation state and CAHS expression could influence exosome production, size distribution, and later post-storage stability.

LPS stimulation was introduced to generate M1-like, pro-inflammatory macrophages and corresponding M1-associated exosomes.[24] In contrast, the previously used hypotonic H_2O stimulation was used to stimulate exosomes from M2-like macrophages (anti-inflammatory) and was treated as the comparison condition for exosome release.[24] RAW macrophages were stimulated with 1 µg/mL LPS.[25] To achieve this, LPS powder derived from E. coli was prepared in sterile PBS, and 16 µL of LPS stock solution was added to macrophage cultures, followed by 24 hours of incubation before exosome collection. After stimulation, exosomes were collected using the established exosome isolation protocol described previously (Figure 1). This same workflow was applied across LPS-stimulated and H_2O-stimulated conditions to allow comparison between macrophage activation approaches. Isolated pellets were resuspended in 1× PBS and analyzed using DLS to evaluate nanoscale particle size distribution (Figure 14).

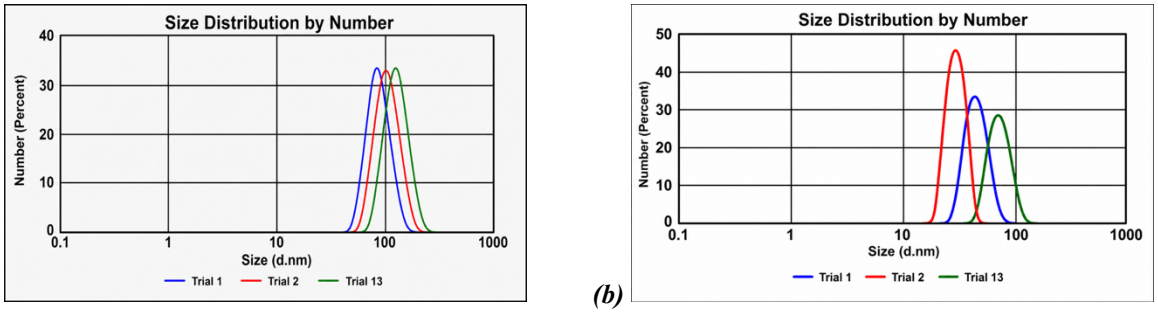

Figure 14. *DLS characterization of control exosomes under different stimulation conditions.*
(a) *DLS size distribution of control exosomes isolated after LPS stimulation, showing the particle size profile of LPS-induced exosome preparations.*
(b) *DLS size distribution of control exosomes generated using hypotonic H_2O stimulation, used to compare size distribution and consistency before post-freeze analysis.*

To reduce contamination from serum-derived extracellular vesicles, later exosome production experiments were performed using DMEM only without FBS prior to collection.[26]

This adjustment helped ensure that measured vesicles were more likely to originate from the macrophage cultures rather than from fetal bovine serum. AcGFP control macrophages and CAHS-associated macrophage systems were prepared for comparative experiments, allowing exosome isolation and characterization across control and protein-associated conditions.

LPS stimulation was then extended to CAHS-expressing macrophages to evaluate whether CAHS-associated exosomes could be generated under pro-inflammatory stimulation conditions. For this experiment, 16 µL of LPS stock solution was added to CAHS-expressing macrophage cultures along with 9,984 µL DMEM without FBS, followed by 24 hours of incubation. Exosomes were then isolated using the established protocol and analyzed by DLS.

DLS characterization of CAHS-associated exosome samples produced a dominant particle size distribution of approximately ~100 nm, consistent with the expected nanoscale range for exosome-like vesicles (Figure 15). This confirmed that CAHS-associated macrophages could generate isolatable vesicle populations under the tested conditions and provided the basis for later post-freeze stability comparisons.

(a)

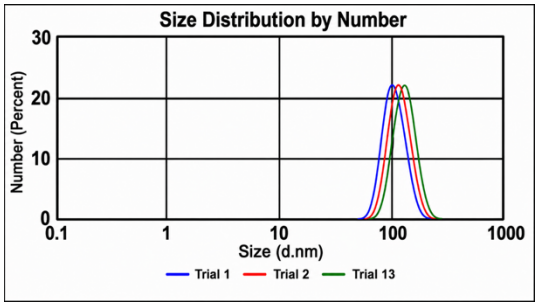

(b)

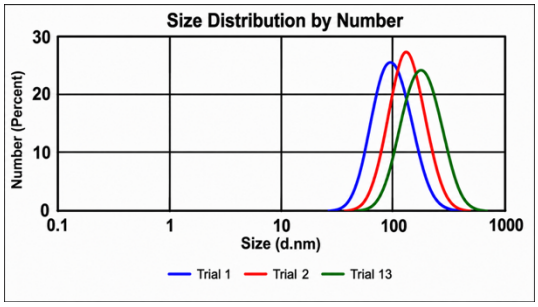

Figure 15. *DLS characterization of CAHS-associated exosomes under different stimulation conditions.*

- ***(a)*** *DLS size distribution of CAHS-associated exosomes isolated after 1 µg/mL LPS stimulation, showing a dominant peak near 147 nm.*
- ***(b)*** *DLS comparison of CAHS-associated exosomes generated using hypotonic H_2O stimulation, used to evaluate differences in size distribution and consistency before post-freeze analysis.*

Overall, Winter 2026 established the comparative framework for evaluating exosomes generated under LPS-stimulated and H_2O-stimulated conditions, while also incorporating CAHS-

associated macrophages into the exosome production system. These experiments set up the later Spring 2026 post-storage comparisons examining whether CAHS expression, LPS stimulation, and storage conditions improved exosome stability after freezing.

Post-Storage Characterization and Comparative Stability Analysis (Spring 2026)

During Spring 2026, experimental efforts focused on post-storage characterization of exosome samples generated during Fall 2025 and Winter 2026. This phase evaluated whether storage condition, stimulation method, and CAHS association influenced exosome stability after freezing. The primary goal was to compare post-freeze particle size distributions across control and CAHS-associated exosome systems using DLS.

In Week 3, stored exosome samples were retrieved and prepared for post-freeze analysis. These samples included control exosomes derived from mScarlet- and AcGFP-expressing macrophages, CAHS-associated exosomes generated under hypotonic H_2O stimulation, CAHS-associated exosomes generated under LPS stimulation, and AcGFP exosomes stored under PBS or sucrose-based cryoprotectant conditions. Each sample was thawed and analyzed using a Zetasizer to assess whether post-freeze particles remained within the expected exosome size range.

The comparative analysis was organized around three major variables: CAHS association versus control, LPS stimulation versus H_2O stimulation, and sucrose storage versus PBS storage. Control samples, including mScarlet- and AcGFP-derived exosomes, were used to evaluate baseline post-freeze stability in the absence of CAHS-associated stabilization. CAHS-associated samples were analyzed to determine whether CAHS expression was associated with improved preservation of nanoscale vesicle size after freezing. LPS- and H_2O-stimulated samples were compared to assess whether macrophage stimulation condition influenced post-storage size

distribution, while PBS- and sucrose-stored AcGFP samples were compared to evaluate the effect of cryoprotective storage.

DLS measurements were used to generate size distribution profiles for each condition (Figures 16-19). Dynamic light scattering (DLS) measurements were performed using a Zetasizer to assess particle size distribution following storage. For each condition, exosome samples were loaded into measurement cuvettes, and size distributions were recorded and saved for subsequent comparison. Measurements were repeated where necessary to ensure consistency and reproducibility of recorded values. Post-freeze control exosomes showed evidence of reduced structural preservation, including loss of expected exosome-sized particle populations or broader size variability. In contrast, CAHS-associated exosome samples retained particle distributions closer to the expected nanoscale exosome range, supporting the role of CAHS-associated stabilization in preserving vesicle structure after freezing. Sucrose-stored samples were also compared with PBS-stored samples to assess whether cryoprotection improved post-freeze size preservation.

All measurements conducted during this phase were performed under consistent instrument settings to ensure comparability across datasets. The resulting size distributions provided a basis for evaluating exosome stability following storage and for comparing the effects of different preparation and preservation conditions across experimental groups.

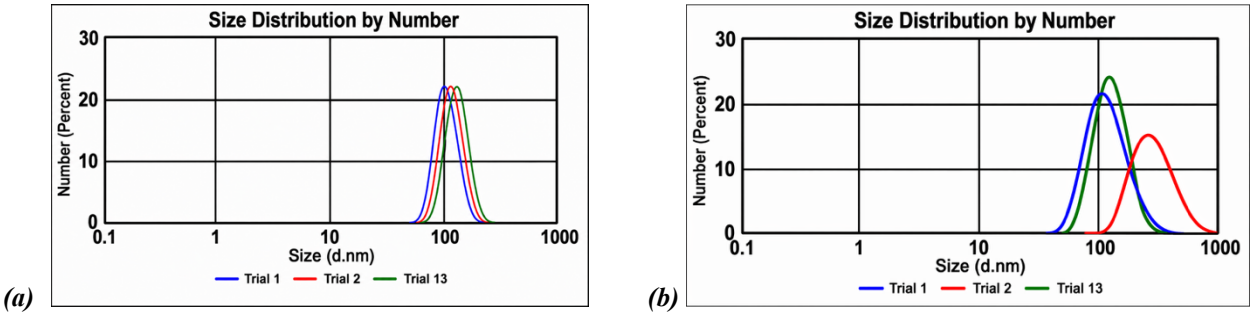

Figure 16. *CAHS-expressing exosomes following LPS stimulation.*

(a) *Pre-freeze DLS size distribution of CAHS-associated exosomes generated after LPS stimulation, showing a narrow and relatively uniform particle profile within the expected exosome range.*
(b) *Post-freeze DLS size distribution of the same CAHS-associated exosome condition, demonstrating retention of a uniform nanoscale particle distribution with reduced evidence of aggregation.*

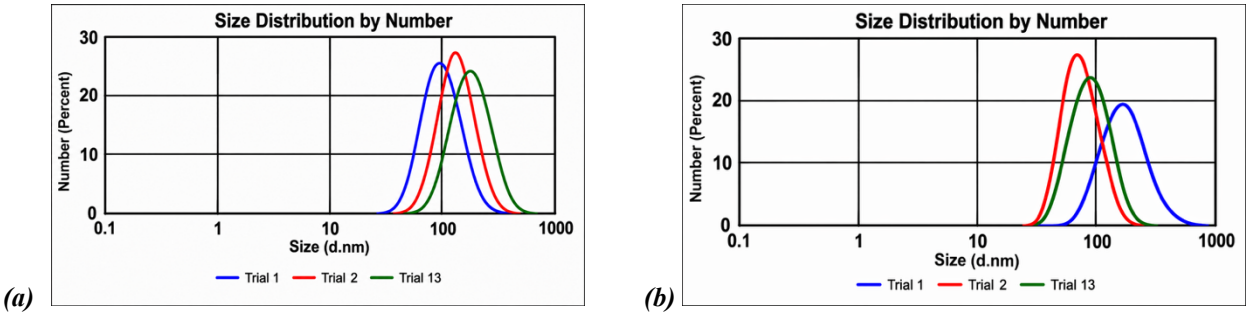

Figure 17. *CAHS-expressing exosomes following hypotonic H_2O stimulation.*
(a) *Pre-freeze DLS size distribution of CAHS-associated exosomes generated after hypotonic H_2O stimulation, showing particles within the expected exosome size range of approximately 30-150 nm.*
(b) *Post-freeze DLS size distribution of the same CAHS-associated exosome condition, showing preservation of the exosome-sized particle population with minimal aggregation.*

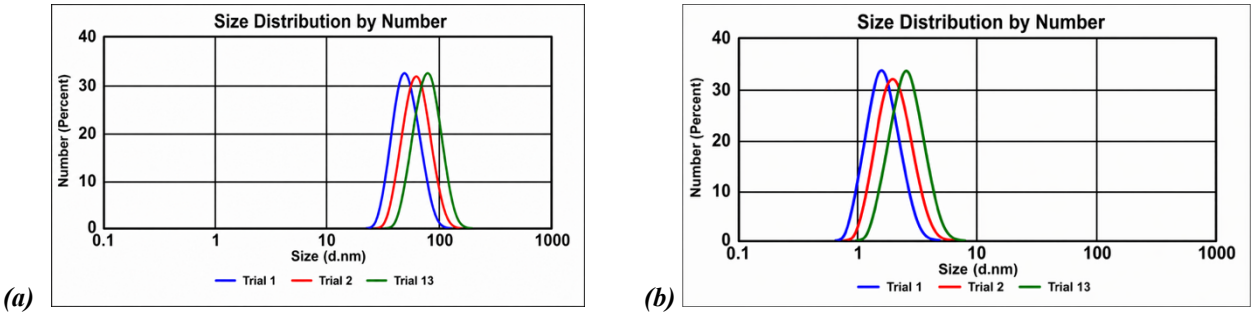

Figure 18. *Control mScarlet exosomes following hypotonic H_2O stimulation.*
(a) *Pre-freeze DLS size distribution of control mScarlet exosomes generated after hypotonic H_2O stimulation, showing a particle profile consistent with expected exosome-sized vesicles.*
(b) *Post-freeze DLS size distribution of the same control condition, showing increased polydispersity and larger particle populations, consistent with aggregation and reduced post-freeze structural stability.*

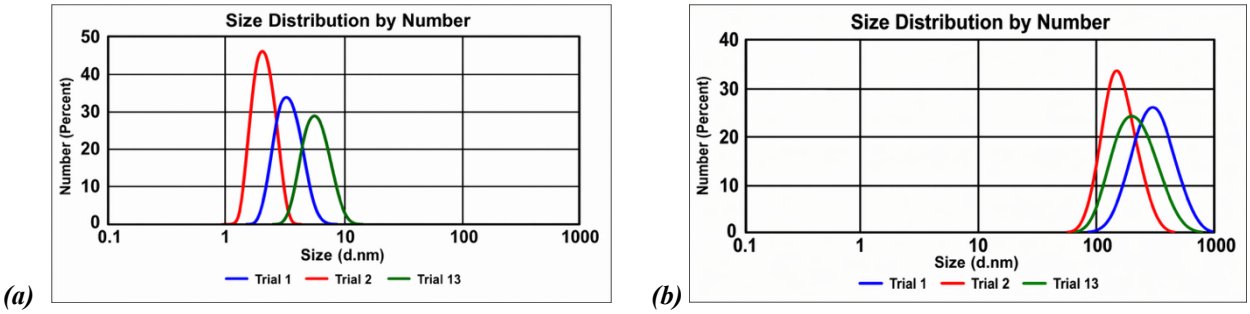

Figure 19. *DLS size distribution of control AcGFP exosomes post-freeze* ***(a)*** *stored in PBS and* ***(b)*** *stored in sucrose-based cryoprotectant conditions, showing improved preservation of nanoscale particle size distribution in sucrose compared to PBS storage.*

CONCLUSION

This project initially focused on optimizing indocyanine green (ICG) loading into immune cells for potential imaging and photothermal applications. Although ICG was successfully loaded into RAW macrophages and monocytes, absorbance, fluorescence, and time-resolved analyses showed that the dye was not stably retained. Instead, intracellular signal decreased over time while ICG accumulated in the surrounding media, demonstrating that passive intracellular loading was insufficient for sustained delivery.

These findings shifted the focus toward macrophage-derived exosomes as a more practical delivery platform. Exosome-like vesicles were successfully isolated using hypotonic stimulation and ultracentrifugation, but post-storage analysis showed that vesicle stability remained a major limitation. Control exosomes exhibited structural disruption and increased variability after freezing, indicating that isolation alone was not enough to preserve vesicle integrity.

To address this, the project explored stabilization strategies, including sucrose-based cryoprotection and CAHS protein incorporation. Sucrose improved post-freeze preservation compared with PBS, while CAHS-associated exosomes maintained size distributions closer to intact exosome-sized particles after freezing. These results suggest that the most relevant contribution of this project is not only ICG loading, but the development of more stable exosome systems for transport, storage, and future payload delivery.

Future work should focus on directly validating exosome morphology using scanning electron microscopy (SEM) and transmission electron microscopy (TEM), optimizing CAHS incorporation, and testing how CAHS proteins preserve vesicle structure. Additional studies

should evaluate direct ICG loading into isolated exosomes, measure ICG retention and release under physiological conditions, and test targeting using tumor models such as SK-OV-3 ovarian cancer cells. Photothermal experiments should also be performed to determine whether stabilized ICG-loaded exosomes can improve localized heating and therapeutic effect. Finally, additional cryoprotectants, freeze-drying methods, long-term storage conditions, and combinations of LPS-induced exosome production with CAHS stabilization should be tested to further improve exosome yield, stability, and translational potential.

REFERENCES

1. Brancewicz J, Wójcik N, Zuzanna Sarnowska, Robak J, Król M. The Multifaceted Role of Macrophages in Biology and Diseases. International Journal of Molecular Sciences. 2025;26(5):2107-2107. doi:https://doi.org/10.3390/ijms26052107
2. Lin Y, Anderson JD, Lily, Gu SV, Knowlton AA. Exosomes in disease and regeneration: biological functions, diagnostics, and beneficial effects. American journal of physiology Heart and circulatory physiology. 2020;319(6):H1162-H1180. doi:https://doi.org/10.1152/ajpheart.00075.2020
3. Tseng HC, Kuo C, Liao W, Chou TS, Hsiao J. Indocyanine green as a near-infrared theranostic agent for ferroptosis and apoptosis-based, photothermal, and photodynamic cancer therapy. Frontiers in Molecular Biosciences. 2022;9. doi:https://doi.org/10.3389/fmolb.2022.1045885
4. Gasperi AD, Mazza E, Prosperi M. Indocyanine green kinetics to assess liver function: Ready for a clinical dynamic assessment in major liver surgery? World Journal of Hepatology. 2016;8(7):355. doi:https://doi.org/10.4254/wjh.v8.i7.355
5. Choi MR, Stanton-Maxey KJ, Stanley JK, et al. A Cellular Trojan Horse for Delivery of Therapeutic Nanoparticles into Tumors. Nano Letters. 2007;7(12):3759-3765. doi:https://doi.org/10.1021/nl072209h
6. Sheng Z, Hu D, Zheng M, et al. Smart Human Serum Albumin-Indocyanine Green Nanoparticles Generated by Programmed Assembly for Dual-Modal Imaging-Guided Cancer Synergistic Phototherapy. ACS Nano. 2014;8(12):12310-12322. doi:https://doi.org/10.1021/nn5062386

7. Kalluri R, LeBleu VS. The biology, function, and Biomedical Applications of Exosomes. Science. 2020;367(6478). doi:https://doi.org/10.1126/science.aau6977
8. Guarro M, Suñer F, Lecina M, Borrós S, Fornaguera C. Efficient extracellular vesicles freeze-dry method for direct formulations preparation and use. Colloids and Surfaces B: Biointerfaces. 2022;218:112745. doi:https://doi.org/10.1016/j.colsurfb.2022.112745
9. Jeyaram A, Jay SM. Preservation and Storage Stability of Extracellular Vesicles for Therapeutic Applications. The AAPS Journal. 2017;20(1). doi:https://doi.org/10.1208/s12248-017-0160-y
10. Schaafsma BE, Mieog JSD, Hutteman M, et al. The clinical use of indocyanine green as a near-infrared fluorescent contrast agent for image-guided oncologic surgery. Journal of Surgical Oncology. 2011;104(3):323-332. doi:https://doi.org/10.1002/jso.21943
11. Alander JT, Kaartinen I, Laakso A, et al. A Review of Indocyanine Green Fluorescent Imaging in Surgery. International Journal of Biomedical Imaging. 2012;2012. doi:https://doi.org/10.1155/2012/940585
12. Wang H, Li X, Tse BWC, et al. Indocyanine green-incorporating nanoparticles for cancer theranostics. Theranostics. 2018;8(5):1227-1242. doi:https://doi.org/10.7150/thno.22872
13. Hill TK, Abdulahad A, Kelkar SS, et al. Indocyanine green-loaded nanoparticles for image-guided tumor surgery. Bioconjug Chem. 2015;26(2):294-303. doi:10.1021/bc5005679
14. van Niel G, D'Angelo G, Raposo G. Shedding light on the cell biology of extracellular vesicles. Nat Rev Mol Cell Biol. 2018 Apr;19(4):213-228. doi: 10.1038/nrm.2017.125. Epub 2018 Jan 17. PMID: 29339798.

15. Zeng H, Guo S, Ren X, Wu Z, Liu S, Yao X. Current Strategies for Exosome Cargo Loading and Targeting Delivery. Cells. 2023;12(10):1416. Published 2023 May 17. doi:10.3390/cells12101416

16. Alvarez-Erviti L, Seow Y, Yin H, Betts C, Lakhal S, Wood MJ. Delivery of siRNA to the mouse brain by systemic injection of targeted exosomes. Nat Biotechnol. 2011;29(4):341-345. doi:10.1038/nbt.1807

17. Liu L, Zhang S, Ren Y, et al. Macrophage-derived exosomes in cancer: a double-edged sword with therapeutic potential. J Nanobiotechnology. 2025;23(1):319. Published 2025 Apr 26. doi:10.1186/s12951-025-03321-1

18. Livshits MA, Khomyakova E, Evtushenko EG, et al. Isolation of exosomes by differential centrifugation: Theoretical analysis of a commonly used protocol. Sci Rep. 2015;5:17319. Published 2015 Nov 30. doi:10.1038/srep17319

19. Ahmadian S, Jafari N, Tamadon A, Ghaffarzadeh A, Rahbarghazi R, Mahdipour M. Different storage and freezing protocols for extracellular vesicles: a systematic review. Stem Cell Res Ther. 2024;15(1):453. Published 2024 Nov 26. doi:10.1186/s13287-024-04005-7

20. Bosch S, de Beaurepaire L, Allard M, et al. Trehalose prevents aggregation of exosomes and cryodamage. Scientific Reports. 2016;6(1). doi:https://doi.org/10.1038/srep36162

21. Tanaka A, Nakano T, Watanabe K, et al. Stress-dependent cell stiffening by tardigrade tolerance proteins that reversibly form a filamentous network and gel. PLoS Biol. 2022;20(9):e3001780. Published 2022 Sep 6. doi:10.1371/journal.pbio.3001780

22. Kurian TK, Banik S, Gopal D, Chakrabarti S, Mazumder N. Elucidating Methods for Isolation and Quantification of Exosomes: A Review. Mol Biotechnol. 2021;63(4):249-266. doi:10.1007/s12033-021-00300-3

23. Geurts, Aron M, et al. "Gene Transfer into Genomes of Human Cells by the Sleeping Beauty Transposon System." Molecular Therapy, vol. 8, no. 1, 1 July 2003, pp. 108–117, www.sciencedirect.com/science/article/pii/S1525001603000996, https://doi.org/10.1016/S1525-0016(03)00099-6. Accessed 14 Mar. 2022.

24. Orecchioni, Marco, et al. "Macrophage Polarization: Different Gene Signatures in M1(LPS+) vs. Classically and M2(LPS–) vs. Alternatively Activated Macrophages." Frontiers in Immunology, vol. 10, 24 May 2019, https://doi.org/10.3389/fimmu.2019.01084.

25. Sui X, Liu W, Liu Z. Exosomes derived from LPS-induced MHs cells prompted an inflammatory response in sepsis-induced acute lung injury. Respiratory Physiology & Neurobiology. 2021;292:103711. doi:https://doi.org/10.1016/j.resp.2021.103711

26. Shelke GV, Lässer C, Gho YS, Lötvall J. Importance of exosome depletion protocols to eliminate functional and RNA-containing extracellular vesicles from fetal bovine serum. Journal of Extracellular Vesicles. 2014;3(1):24783. doi:https://doi.org/10.3402/jev.v3.24783